JARO 13: 249–267 (2012)
DOI: 10.1007/s10162-011-0300-5

JARO
Journal of the Association for Research in Otolaryngology

A Modeling Study of the Responses of the Lateral Superior Olive to Ipsilateral Sinusoidally Amplitude-Modulated Tones

Le Wang[1], and H. Steven Colburn[1]

[1]*Department of Biomedical Engineering, Center for Hearing Research, Boston University, Boston, MA 02215, USA*

Received: 3 January 2011; Accepted: 25 October 2011; Online publication: 13 December 2011

ABSTRACT

The lateral superior olive (LSO) is a brainstem nucleus that is classically understood to encode binaural information in high-frequency sounds. Previous studies have shown that LSO cells are sensitive to envelope interaural time difference in sinusoidally amplitude-modulated (SAM) tones (Joris and Yin, J Neurophysiol 73:1043–1062, 1995; Joris, J Neurophysiol 76:2137–2156, 1996) and that a subpopulation of LSO neurons exhibit low-threshold potassium currents mediated by Kv1 channels (Barnes-Davies et al., Eur J Neurosci 19:325–333, 2004). It has also been shown that in many LSO cells the average response rate to ipsilateral SAM tones decreases with modulation frequency above a few hundred Hertz (Joris and Yin, J Neurophysiol 79:253–269, 1998). This low-pass feature is not directly inherited from the inputs to the LSO since the response rate of these input neurons changes little with increasing modulation frequency. In the current study, an LSO cell model is developed to investigate mechanisms consistent with the responses described above, notably the emergent rate decrease with increasing frequency. The mechanisms explored included the effects of after-hyperpolarization (AHP) channels, the dynamics of low-threshold potassium channels (KLT), and the effects of background inhibition. In the model, AHP channels alone were not sufficient to induce the observed rate decrease at high modulation frequencies. The model also suggests that the background inhibition alone, possibly from the medial nucleus of the trapezoid body, can account for the small rate decrease seen in some LSO neurons, but could not explain the large rate decrease seen in other LSO neurons at high modulation frequencies. In contrast, both the small and large rate decreases were replicated when KLT channels were included in the LSO neuron model. These results support the conclusion that KLT channels may play a major role in the large rate decreases seen in some units and that background inhibition may be a contributing factor, a factor that could be adequate for small decreases.

Keywords: LSO, low-threshold potassium channel, auditory brainstem, cochlear nucleus bushy cells, envelope processing

INTRODUCTION

The lateral superior olive (LSO) is the first nucleus in the ascending auditory pathway that encodes binaural level information (Boudreau and Tsuchitani 1968; Finlayson and Caspary 1991; Tollin and Yin 2005). LSO cells receive excitatory inputs from the spherical bushy cells (SBCs) of the ipsilateral anteroventral cochlear nucleus (AVCN) and inhibitory inputs from the globular bushy cells in the contralateral VCN via the ipsilateral medial nucleus of the trapezoid body (MNTB) (Smith et al. 1991, 1993, 1998). Due to this excitation–inhibition (EI) interaction, it is not surprising that LSO cells are sensitive to interaural level differences (ILDs). Previous studies have also shown that LSO cells are sensitive to interaural time differences in the envelopes of sinusoidally amplitude-modulated (SAM) tones (Joris and Yin 1995; Batra et al. 1997). Again, this sensitivity is expected for an EI cell whose inputs are synchronized to the envelopes of the filtered input waveforms.

Correspondence to: H. Steven Colburn · Department of Biomedical Engineering, Center for Hearing Research · Boston University · Boston, MA 02215, USA. colburn@bu.edu

While LSO responses to binaural SAM tones could largely be explained by the interaction between excitation and inhibition (Joris 1996), the responses to monaural SAM tones are less well understood. Specifically, the firing rate of LSO cells in response to ipsilateral SAM tones generally decreases rapidly with the increase in the modulation frequency (Joris and Yin 1998). In 12 of 13 LSO units shown in Figure 1B, for example, the firing rate decreased with increasing modulation frequency (f_m). However, the magnitude of the rate decrease and the firing rate at the highest modulation frequency varied among units.

One might hypothesize that the low-pass rate tuning for modulation frequency is inherited from the LSO afferents, specifically the SBCs; however, the firing rates in the SBCs are more stable with respect to modulation frequency than the firing rates in the LSO, as shown in Figure 1. The rate decrease in the SBC units is generally less than 50 spikes/s; therefore, the large rate decrease observed in most LSO cells is unlikely to be directly inherited from the SBCs. Another possible mechanism to explain the rate decrease in the LSO was suggested by Joris and Yin (1998). They suggested that the baseline inhibition in the LSO, derived from spontaneous activity in the ipsilateral MNTB, might suppress the sustained excitatory input at high modulation frequencies more effectively than the modulated excitatory input at low modulation frequencies. However, no quantitative LSO model has been built to test the effect of the baseline inhibition on the f_m-dependent firing rate.

Another feature of the responses in the LSO to ipsilateral SAM tones is that phase locking to the envelope becomes weaker at higher modulation frequencies. The degree of phase locking to the envelope is characterized by vector strength (Goldberg and Brown 1969), also known as synchronization index (SI). The SI varies from zero for homogenous spike distribution across the stimulus period to unity for perfect phase locking when all spikes occur at the same stimulus phase. The temporal modulation transfer function (tMTF) is typically used to illustrate the dependence of the SI on the modulation frequency. Temporal MTFs for most LSO cells have low-pass characteristics, a feature referred to as "envelope filtering". tMTFs for LSO cells largely resemble those for SBCs with a few minor differences. When compared with the SBC, LSO cells show higher maximum synchronization and lower 3-dB cutoff frequency in their tMTFs (Joris and Yin 1998). As illustrated in the simulations presented below, these temporal transformations naturally arise in the LSO model in the attempt to reproduce the firing rate decrease with frequency in LSO cells described above. Therefore, the present study focuses on reproducing the firing rate vs. modulation frequency relationship in the monaurally stimulated LSO. After the rate–f_m function was reproduced in the LSO model, the tMTF was computed in the same LSO model only to confirm that the LSO model in the present study was able to explain both the average rate and the synchronization of the LSO responses to monaural SAM tones.

While a number of LSO models have been developed over the past few decades, none of them have sought to reproduce the LSO responses to SAM tones. Some modeling studies characterized the ILD encoding in the average rate of the LSO responses to binaural stimuli (Colburn and Moss 1981; Johnson et al. 1990; Reed and Blum 1990; Blum and Reed 1991) and are unlikely to explain the LSO response to monaural SAM tones. Two other modeling studies characterized temporal aspects of spike trains produced by LSO neurons in response to monaural, noise, or tone burst stimulation (Zacksenhouse et al. 1998; Zhou and Colburn 2010) and could potentially be applied to describe the responses to monaural SAM tones. Because these two LSO models were modeling similar temporal features, notably the serial dependence between adjacent spike intervals, with similar mechanisms, we chose to test the less complex model, developed in Zhou and Colburn (2010). A key component for the serial dependence in these models

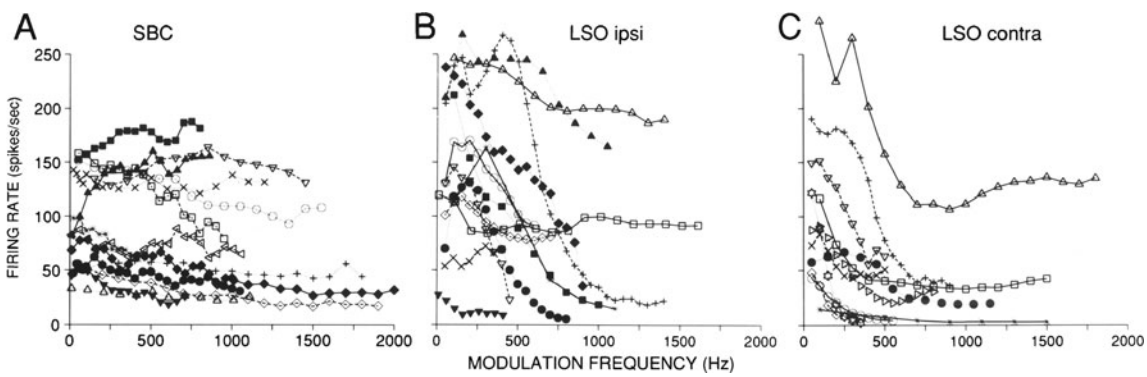

FIG. 1. Average firing rate plotted as a function of modulation frequency for spherical bushy cells (**A**) and LSO units (**B**: ipsilateral modulation; **C**: contralateral modulation). Different curves in each panel represent different units [figure from Joris and Yin (1998)].

was an after-hyperpolarization (AHP) channel. The extent to which this channel also contributes to the rate–f_m relation in the LSO response to SAM tones is examined in the present study.

Also considered were models developed to explain the f_m-dependent firing rate in response to monaural SAM tones in the IC. For various reasons, none of these models appears suitable to explain the rate–f_m behavior in the LSO. For example, an IC model shows that the band-pass-shaped temporal MTF function of the chopper units in VCN may be translated into band-pass-shaped rate–f_m function if the IC cells act as coincidence detectors (Hewitt and Meddis 1994). Another IC model used the convergence of inhibition and excitation as a mechanism for creating band-pass rate tuning for the modulation frequency (Nelson and Carney 2004). However, neither excitatory inputs from VCN chopper units nor inhibitory inputs that phase lock to the stimulus envelope have been found in the cat LSO with monaural stimulation, making the above mechanisms in the IC unlikely to explain the LSO data in Figure 1B.

In the present study, computational modeling is used to explore several mechanisms that might explain the low-pass rate tuning for the modulation frequency in the LSO. In addition to the AHP mechanism and the baseline inhibition effects described above, a third hypothesis, that the low-threshold potassium (KLT) channel in the LSO cell membrane reduces the firing rate as the modulation frequency increases, is also considered. This hypothesis, also referred to as the KLT hypothesis, is suggested by the observations that activated KLT channels suppress the ongoing discharges in AVCN bushy cells (Rothman and Manis 2003a, b, c) and that KLT channels are present in the rat LSO cell membrane (Barnes-Davies et al. 2004). If the KLT channels in the LSO remain activated during SAM tone stimulation at high modulation frequencies, one would expect that the ongoing discharges would be suppressed and the firing rate would be reduced.

This paper analyzes several model structures, with variable parameters. First, the behavior of the LSO model developed in Zhou and Colburn (2010) in response to SAM tones is explored and the effect of the AHP channel on the firing rate is discussed. Second, a new (Hodgkin–Huxley-type) LSO model is used to test other possible mechanisms that might explain the dependence of the firing rate on the modulation frequency, particularly the firing rate decrease at high modulation frequency. This new LSO model specifically includes either KLT channels or background inhibition, both potential mechanisms for explaining LSO responses to SAM tones. The KLT conductance, the firing rate of the synaptic inputs, and the number of the synaptic inputs were varied to examine their effects on the average firing rate of the model in response to SAM tones.

METHODS

Cell models

Two types of LSO cell models are presented in this study. The first is based on a modified leaky integrate-and-fire (LIF) model (Zhou and Colburn 2010). This model structure contains only a capacitance c_m, a leak conductance g_{leak}, and two time-varying conductance-based channels G_{abs} and $g_{AHP}(t)$ that control absolute and relative refractory behavior. Spikes are generated in the model in response to each occurrence of the membrane potential reaching a fixed threshold V_{th}. Following the spike time t_n, the membrane potential was fixed at the resting potential (V_{rest}) by a large shunting conductance G_{abs} for the duration T_{abs}. After the time T_{abs}, the AHP channel conductance $g_{AHP}(t)$ was increased by a fixed amount G_{AHP} and decayed exponentially toward zero with a time constant τ_{abs}. The parameters of this cell model were taken from Zhou and Colburn (2010) and are summarized in Table 1.

The second type of cell model used here is a Hodgkin–Huxley (HH) model. In comparison with the LIF model, although the HH model is more complicated with the inclusion of voltage-dependent conductances, it allows the evaluation of the effects of KLT channels as previously described and is also more physiological. This LSO model was implemented using NEURON (Hines and Carnevale 1997), a broad purpose, neuron simulation environment. The HH-type LSO cell model that we used was a single compartment model with several ion channels in the membrane: a sodium channel, a "leak" channel, a high-threshold potassium channel (KHT) and a KLT channel. These ion channels, which are believed to be present in LSO cell membranes, are modeled with mathematical characterizations based on those channels empirically described for AVCN cells (Rothman and Manis 2003a, b, c). Finally, for more direct comparisons, the HH-type LSO model shares the same passive membrane properties (g_{leak} and c_m) with the LIF-type LSO model.

In the studies presented here, the basic structure for the HH-type LSO cell model (cf., Fig. 2) was fixed while channel parameters were varied.

TABLE 1

Membrane properties for the LIF model for LSO

	Cell 1	*Cell 2*	*Cell 3*	*Cell 4*
G_{AHP} (μS)	0.02	0.05	0.02	0.08
τ_{AHP} (ms)	20	20	5	5

$\boldsymbol{c_m}$=31.4 pF; $\boldsymbol{g_{leak}}$=0.0314 μS; $\boldsymbol{\tau_m}=\boldsymbol{c_m}/\boldsymbol{g_{leak}}$=1 ms; $\boldsymbol{g_{abs}}$=10 μS; $\boldsymbol{T_{abs}}$=2 ms; $\boldsymbol{E_{leak}}=\boldsymbol{E_{AHP}}=\boldsymbol{E_{abs}}=\boldsymbol{V_{rest}}$=−65 mV; $\boldsymbol{V_{th}}$=−50 mV

MATLAB (MathWorks, Natick, MA, USA) was used to initialize the LSO model parameters before each simulation and to organize the results after each simulation. In particular, the peak conductance of the KLT channel, g_{KLT}, was varied to investigate its effect on the average firing rate in response to SAM tones. The overall membrane time constant τ_m and the membrane resistance r_m, which are used to interpret some of the results, were computed as follows: The membrane resistance r_m is equal to the combined resistance of all channels at rest. It was computed as the reciprocal of the sum of all the membrane conductances at resting potential (around −65 mV in the model). The resting conductance is principally attributed to the leak channel conductance g_{leak}. A small amount of resting conductance is attributed to the slight KLT channel opening. Sodium channel and KHT channel conductance did not contribute because they were inactive at rest. The circuit diagram of the LSO cell model is shown in Figure 2 with default parameter values given in Table 2. The excitatory and inhibitory synaptic inputs shown in Figure 2 will be described in the following section.

Current and synaptic stimuli

Three types of inputs were used to stimulate the LSO cell models: an external current injection, a synaptic input model driven by a point-process auditory nerve (AN) description, and a synaptic input model driven by a detailed AN model that incorporates physiologically realistic cochlear processing. By using an AN model for the inputs, the CN was essentially treated as relay for the sake of simplicity. For all three types of inputs, the duration of the stimulus was 600 ms with no onset or offset ramping.

The first type of input was an external current injection that simulates the synaptic current generated by an ipsilateral (excitatory) SAM tone. This input was only used to stimulate the LIF-type LSO model. The input current, denoted by I_e, is computed as the sum of a sinusoidal current and a zero mean, constant variance Gaussian noise current I_{noise}. Specifically, the equation that describes the I_e during the stimulus is:

$$I_e = I_{mean}(1 + \sin(2\pi f_m t)) + I_{noise} \quad (1)$$

The frequency f_m of the sinusoidal current represents the modulation frequency of the SAM tone. The modulation depth of the input current is always 100%, and the mean value of the sinusoidal current is denoted by a separate parameter I_{mean}. Note that I_e is held at zero in the intervals before and after the stimulus. Also note that when f_m=0 Hz, the sinusoidal current becomes a noisy current step with amplitude I_{mean}. This current step simulates the excitatory synaptic current generated by a high-frequency pure tone.

The second type of input was generated from a simplified AN model based on a Poisson point process. The rate function of the Poisson process for a single ipsilateral (excitatory) AN fiber is a sinusoidal function described by:

$$\text{rate}_E = \text{rate}_{mean}(1 + \sin(2\pi f_m t)) \quad (2)$$

where f_m represents the modulation frequency of the SAM tone. Multiple ipsilateral AN fibers with the same rate function were used to provide excitatory inputs to the LSO model. When an inhibitory input was used, unless otherwise noted, the rate function of the Poisson process for a single inhibitory input (rate_I) is a constant and represents the spike rate for the spontaneous activity of the ipsilateral MNTB. Each spike generated by the AN model elicits a postsynaptic conductance (PSC), and the total synaptic conductance waveform (excitatory or inhibitory) was computed as the sum of all the corresponding PSCs during the stimulus.

The third type of input was based on a detailed AN model provided by Earlab (http://earlab.bu.edu). Earlab is a collection of implemented auditory models

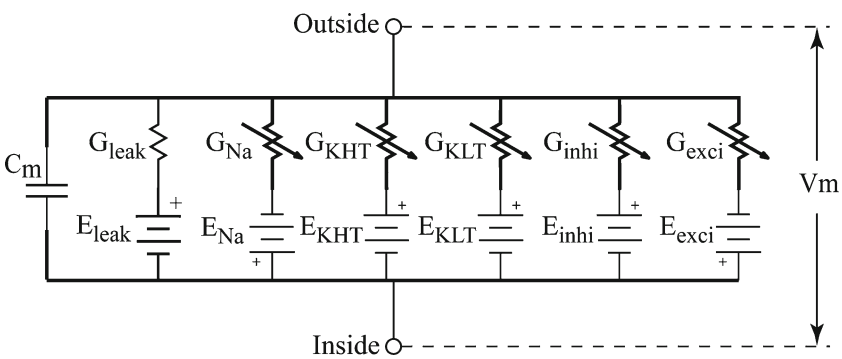

FIG. 2. Circuit diagram for the HH-type LSO cell model with four non-synapse channels: leak channel, sodium channel (*Na*), low-threshold potassium channel (*KLT*), and high-threshold potassium channel (*KHT*). The other two channels, G_{exci} and G_{inhi}, represent excitatory and inhibitory synaptic inputs.

TABLE 2

Membrane properties of the HH-type LSO model

c_m	V_{rest}	g_{leak}	g_{Na}	g_{KHT}	g_{KLT}	E_{leak}	E_{Na}	E_K
31.4 pF	−65 mV	31.4 nS	8,000 nS	1,200 nS	Varied	−65 mV	0 mV	−70 mV

and data analysis software tools (modules). The detailed AN model used in the present study combines a series of models that simulate different stages of auditory processing (Carney 1993; Mountain and Cody 1999; Lopez-Poveda and Meddis 2001). This model is most realistic among the three types of input models used here in that it includes envelope filtering and is driven by acoustic inputs (fully modulated SAM tones. The action potentials generated by the Earlab AN model were then transmitted to the LSO cell model through the same synapses described above. In simulations for ipsilateral modulation, this detailed model was only used for the excitatory inputs while the inhibitory inputs, when used, were always constant rate Poisson processes.

For both the simplified AN model and the detailed AN model, the synaptic conductance for each input was simulated as a linear combination of two exponentials with excitatory and inhibitory peak conductances specified ($\mathrm{str_E}$ and $\mathrm{str_I}$, respectively). [Single-exponential-shaped PSCs were also tested in the model and the shape of the PSC did not significantly affect the simulation result (results not shown).] Specifically, each excitatory PSC was expressed as

$$g(t) = \frac{\mathrm{str_E}}{g_{\mathrm{norm}}}\left[\exp(-t/\tau_{\mathrm{E}}) - \exp(-t/\tau_{\mathrm{E\_rise}})\right] \qquad (3)$$

where $\tau_{\mathrm{E\_rise}}$ and τ_{E} refer to the rise time constant and decay time constant for excitation. The normalization factor was chosen to be $g_{\mathrm{norm}} = \exp\left(-t_{\mathrm{p}}/\tau_{\mathrm{E}}\right) - \exp\left(-t_{\mathrm{p}}/\tau_{\mathrm{E\_rise}}\right)$ so that the peak conductance for each EPSC was $\mathrm{str_E}$ and the time of the peak was t_{p}, where $t_{\mathrm{p}} = \frac{\tau_{\mathrm{E\_rise}}\tau_{\mathrm{E}}}{\tau_{\mathrm{E}}-\tau_{\mathrm{E\_rise}}}\ln\frac{\tau_{\mathrm{E}}}{\tau_{\mathrm{E\_rise}}}$ with $\tau_{\mathrm{E}} > \tau_{\mathrm{E\_rise}}$. (Inhibition is given in the same form with corresponding parameters $\tau_{\mathrm{I\_rise}}$ and τ_{I}.) If the synaptic input is comprised of N spikes and T_i refers to the time of each spike in the input, then the synaptic conductance is given in the form $\sum_{i=1}^{i=N} g(t - T_i)$, where $g(t)$ is the function describing the PSC. The parameters N_{E} and N_{I} refer to the number of AN cells that send excitatory and inhibitory inputs to the LSO cell model. In the simulations that vary the number of excitatory inputs, the total amount of the synaptic conductance was fixed to eliminate the effect from changing the overall level of the synaptic current. For the sake of simplicity, the total amount of the synaptic conductance was computed as the product of the total number of spikes in the stimulus duration and the peak conductance for the PSC $g(t)$. Default parameters for the input models are given in Table 3. For simulations with the second and third types of inputs, the reversal potential was 0 mV for excitatory synapses and −70 mV for inhibitory synapses.

TABLE 3

The default input parameters (point process AN input and Earlab AN input)

N_E (N_I)	τ_E	τ_{E_rise}	τ_I	τ_{I_rise}	$rate_I$
20	1 ms	0.1 ms	2 ms	0.2 ms	30 spikes/s

RESULTS

Results are presented first for the LIF model of Zhou and Colburn (2010), with the same AHP channel description given in their paper; then, the results for the HH-type model are reviewed. In the "Integrate-and-fire type model with AHP channels" section, cases with the LIF model are considered. This LSO cell model was stimulated first with external current injections and later with synaptic inputs. Then, in the "HH-type LSO model with background inhibition" section, simulations with the HH-type LSO model are used to study the effects of background inhibition. The final cases, presented in the "HH-type LSO model with the KLT channel" section, considered the HH-type LSO cell model with the KLT channel. Inputs from the simplified AN model and the detailed AN model were applied separately in the HH-type LSO model presented in sections "HH-type LSO model with background inhibition" and "HH-type LSO model with the KLT channel". In general, the instantaneous rate for each point process follows the shape of the sinusoidal current used in the LIF model simulations ("Integrate-and-fire type model with AHP channels" section); however, the stochastic input used in the HH-type models is more irregular and may lead to more realistic results.

To describe the rate–f_{m} function efficiently, an empirical parameter called the relative peak height (RPH) was defined as the rate difference between maximum firing rate in the rate–f_{m} function and the firing rate at the highest modulation frequency tested

(1,500 Hz for the model). The RPH and the firing rate at 1,500 Hz were used as the primary parameters to characterize the rate–f_m functions in the results of the model. For purposes of comparison to model responses, the LSO cells in Figure 1B can be separated into two roughly equal-sized groups (seven cells vs. six cells) based on whether their RPH values are greater than 100 spikes/s. It is observed in Figure 1B that the group with large RPH values (greater than 100 spikes/s) tends to exhibit low firing rates (less than 50 spikes/s) at the highest modulation frequencies measured. In contrast, the group with small RPH values (less than 100 spikes/s) tends to show relatively high firing rate at the highest f_m measured (close to or above 100 spikes/s), although with more variability compared with the first group. Based on this observation, when the firing rate at 1,500 Hz in the simulation is low (around 25 spikes/s), a rate–f_m function with a high RPH value (close to or above 100 spikes/s) is considered a good prediction of the empirical data. On the other hand, when the firing rate at 1,500 Hz is high (around 100 spikes/s), there is no restriction on the RPH value for good predictions. Although LSO cells are divided into two RPH groups for these comparisons, the actual distribution of these parameters is not yet clear from the available data.

Integrate-and-fire type model with AHP channels

The first model results described here use the LIF-type LSO model developed in Zhou and Colburn (2010). Specifically, their model cells with four different sets of AHP channel parameters (Table 1) were first stimulated with noisy current steps. We confirmed that all of the model cells showed the chopping behavior they described as well as the negative serial correlations between neighboring inter-spike intervals present in the empirically measured LSO response to pure tones. Then, the same four model cells (cell 1 to cell 4) were simulated with sinusoidal current injections of increasing levels and the results are summarized in Figure 3. The mean current levels used here are similar to those used in Zhou and Colburn (2010).

At the highest current levels, these cells with AHP channels responded to SAM tones at relatively high rates (Fig. 3) and did not show a clear decay in firing rate at high modulation frequencies. Firing rates decreased overall as the current injection level decreased from high to intermediate levels, and peaks in the rate–f_m function began to emerge around 200 to 400 Hz in each of these cells. At intermediate current levels, because the firing rate decreased relatively slowly with increasing modulation frequency up to 1,500 Hz, the peaks in the function took on a broad appearance. In contrast, the slope of the firing rate decay in most LSO units in Figure 1B is much steeper and the steepest slope of the decrease typically occurs below 1,000 Hz. This suggests that the LSO model with AHP channels at intermediate current levels cannot fully reproduce the rate decay measured empirically. At the lowest current level tested (0.3 nA), all of the cells showed a low firing rate at 1,500 Hz and a single peak in the rate–f_m functions around 100 Hz. Among the four example cells, the rate–f_m function of cell 3 showed the largest RPH value (close to 100 spikes/s), which may reflect the fact that cell 3 has the lowest overall level of the AHP conductance (smallest G_{AHP} and τ_{AHP}). In addition to cells 1–4, which are distinguished by their values of G_{AHP} and τ_{AHP}, additional values for G_{AHP} and τ_{AHP} were also tested and the simulation results are similar to those of the example cells just described.

To explore whether the single peak in the rate–f_m function at very low current levels was caused primarily by AHP channel activity, we removed the AHP channel from the LSO model and re-ran the simulation. Because the four example cells differed only in the AHP channel parameters, they became the same cell after the AHP channel was removed. As shown in Figure 4, the LSO model without the AHP channel also produced a single peak in the rate–f_m function at 0.3 nA. At this current level, the RPH without the AHP channel was even higher than that observed in the example cells (cell 1 to cell 4). This result suggests that the AHP channel is not the main cause of the peak in the rate–f_m function at low current levels shown in Figure 3. Further, as current level increased, the rate–f_m function became relatively flat (Fig. 4), indicating that the rate decrease observed at high f_m can only be reproduced at very low current levels in the LIF model.

To summarize, even though the AHP channel in the LIF model generates the chopper response pattern and level-dependent interval statistics of the LSO in response to pure tones, the results presented here suggest that this AHP channel is unlikely to be the primary mechanism that produces the rate decrease in response to SAM tones. The observation that a simple LIF model with only passive membrane properties (leak channel and membrane capacitance) could reproduce the rate decrease in the LSO data at a low current level (Fig. 4) suggests a role for the membrane as a filter. This filtering role can be understood with the following analysis.

During the current injection, the membrane potential $V_m(t)$ can be decomposed into two terms: V_{mean} and $V_{mod}(t)$, where V_{mean} corresponds to the DC response caused by I_{mean} and $V_{mod}(t)$ corresponds to the AC response caused by the modulation current

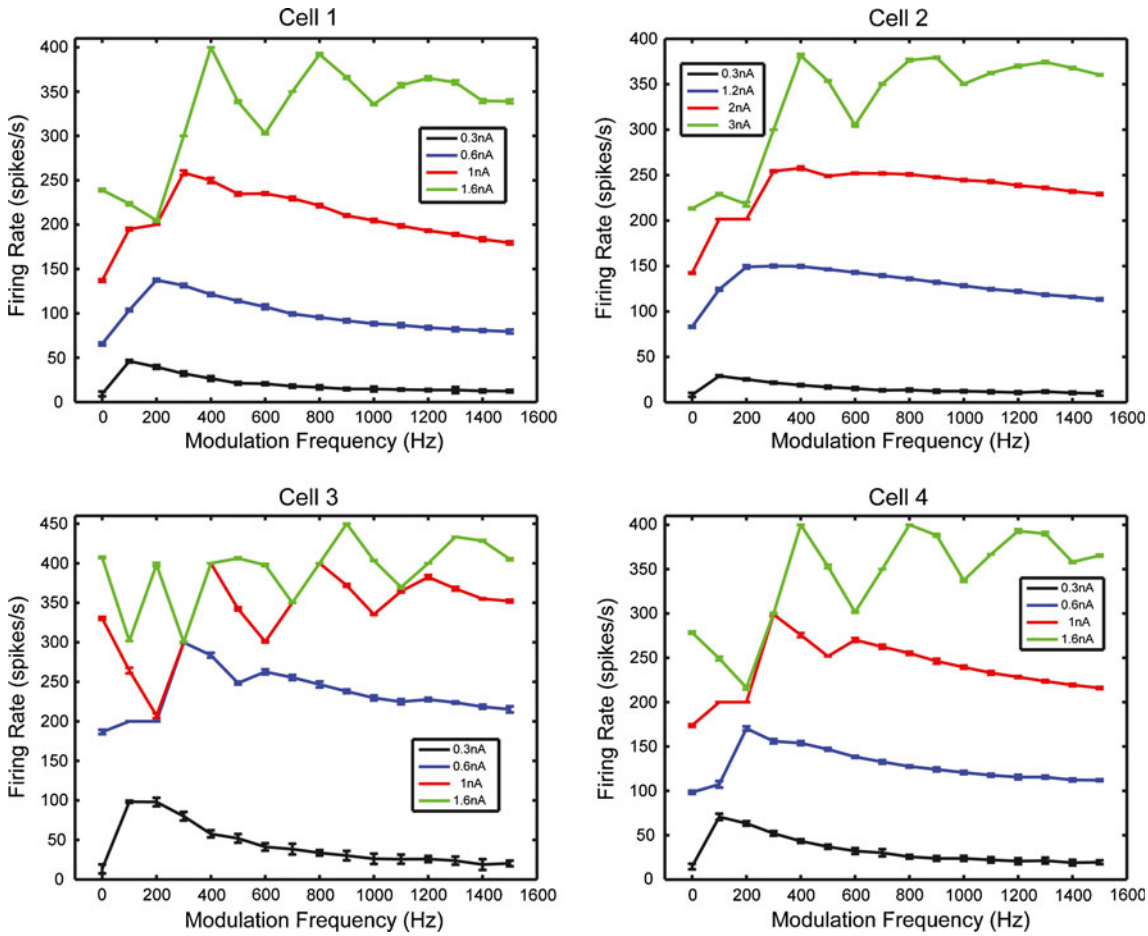

FIG. 3. Rate–f_m functions of example cells for the LIF model as defined in Zhou and Colburn (2010). *Different colors* represent different current injection levels.

$I_{mean}\sin(2\pi f_m t)$. When f_m is zero, $V_m(t)$ equals V_{mean}. Therefore, if V_{mean} is below the firing threshold V_{th}, the cell would not fire when the modulation frequency is zero. For low (but non-zero) values of f_m, $V_m(t)$ equals to $V_{mean}+V_{mod}(t)$. In this case, the peaks in $V_m(t)$ are likely to exceed V_{th}, giving rise to a higher firing rate. As f_m increases, passive membrane filtering would decrease the amplitude of $V_{mod}(t)$ so that, at high f_m, the firing rate would decrease because the peaks in the filtered $V_m(t)$ would decrease below V_{th}. Thus, the firing threshold nonlinearity together with the passive membrane filter could explain why a simple LIF model (no AHP) can generate a single peak in the rate–f_m function.

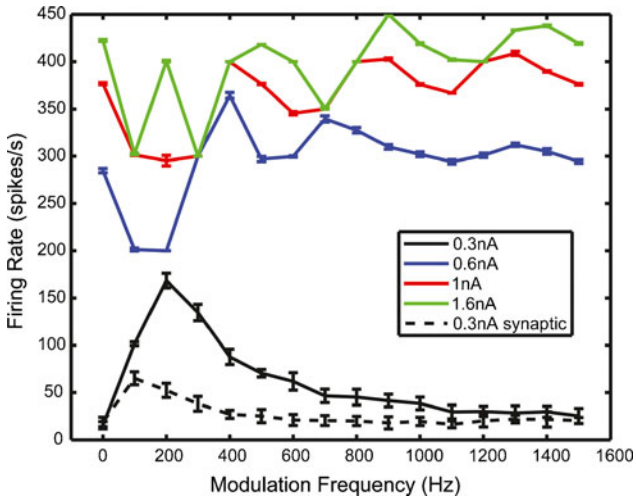

FIG. 4. Rate–f_m functions of the LIF model without the AHP channel. *Solid lines* connect model results with injected currents; *different colors* represent different current injection levels. The *dashed black line* connects model results with synaptic inputs, where $rate_{mean}$=100 spikes/s, str_E=2 nS, and N_E=20.

Even though this simple LIF model looked promising, two important limitations were apparent. First, this model is very sensitive to the overall level of the input (current injection). The rate decay was only reproduced at a current level that was close to the firing threshold. Second, in actual cells, the synaptic current is generally more irregular than the sinusoidal current injection used in the model, which could disrupt the f_m-dependent peak amplitude in $V_m(t)$ created by the passive membrane filter. To test the effect of the randomness in actual synaptic inputs in the simple (no-AHP) LIF model, the current injections were replaced with synaptic inputs driven by a

simplified AN model. In this simulation, the mean level of the synaptic current was chosen to be similar to firing threshold (roughly 0.3 nA). In this case, the peak in the rate–f_m function and the overall variation with rate were significantly reduced (Fig. 4, dashed line). This suggests that this simple, no-AHP LIF model with realistic inputs does not fully explain the observed rate decay in the empirical LSO data (Fig. 1B). Other mechanisms were then considered to reproduce the rate decay in the empirical rate–f_m function of the LSO cell.

HH-type LSO model with background inhibition

As noted previously, another possible mechanism was suggested by Joris and Yin (1998) to explain the low firing rates observed at high modulation frequencies. Specifically, they noted that the MNTB cells on the ipsilateral side of the LSO could provide a base inhibitory input to the LSO due to spontaneous discharges, and this input would block modulated excitatory inputs (at low modulation frequencies) less effectively than sustained excitatory inputs (at high modulation frequencies). We tested this hypothesis with the HH-type LSO model with both excitatory and inhibitory inputs driven by an AN model (either simplified or detailed) with no KLT conductance included.

To explore the effect of the inhibitory inputs on the model's rate–f_m function, the number of inhibitory input (N_I) and the inhibitory synaptic strength (str_I) were varied. The results of the LSO model using the simplified AN model are summarized in Figure 5 (solid lines). The model firing rate was plotted as a function of the modulation frequency when N_I was set to 200 (Fig. 5A) and 20 (Fig. 5B), respectively. For each value of N_I, the excitatory synaptic strength was chosen to produce a relatively high firing rate (250 spikes/s) at zero modulation frequency when no inhibition was present (solid blue curves in Fig. 5A, B). As seen in each panel of Figure 5, when no inhibition was present, the average rates of the LSO model response remained relatively high at all modulation frequencies. For both N_I=20 and N_I=200, rate–f_m functions with two additional levels of inhibition ("weak" and "strong") are shown in Figure 5. The strength str_I of the weak inhibition was chosen to reduce the rate at the highest modulation frequency (1,500 Hz) to around 100 spikes/s, and the str_I of the strong inhibition was chosen to reduce the rate at 1,500 Hz to around 25 spikes/s. These values of the firing rate were chosen to represent the firing rates of the two groups of LSO cells at the highest f_m measured, as previously described in this paper. As expected, when the inhibitory synaptic strength str_I increased from zero, the response rates decreased for all modulation frequencies. When N_I=200 (Fig. 5A), the RHP values of the rate–f_m functions for both weak and strong inhibition were close to 100 spikes/s, approaching the size of the rate decrease in the empirical data (Fig. 1B). When N_I=20 (Fig. 5B), the rate–f_m function showed a much smaller rate variation compared with the case of N_I=200 for both weak and strong inhibition. In particular, the dependence of the firing rate was almost eliminated by the strong inhibition when N_I=20. The results shown in Figure 5 can be understood by considering the level of randomness in the synaptic conductance for the different number of inhibitory inputs. As the input number N_I becomes larger, the synaptic conductance approaches the rate function of the underlying Poisson process because the randomness introduced by each input is reduced due to temporal summation of PSCs. Therefore, the synaptic conductance was very close to a flat function when N_I=200. This constant inhibition, although decreasing the overall level of the excitation, did not significantly disrupt the temporal structure in the excitation that represented the modulation frequency, resulting in a larger rate variation in the rate–f_m function. Conversely, when N_I=20, the observed smaller rate variation is probably due to a higher level of randomness in the inhibitory conductance.

One further issue was addressed in the context of the effects of background inhibition. The results shown in Figure 5 (solid lines) were based on the simplified AN input model which lacked the f_m-dependent synchronization to the envelope. Specifically, in those simulations, the vector strength of the simplified AN inputs was around 0.5, independent of modulation frequency. In actual SBC responses to SAM tones, the phase locking to the envelope becomes weaker at high modulation frequencies (Frisina et al. 1990a; Rhode and Greenberg 1994; Joris and Yin 1998). This envelope filtering might enlarge the rate decrease that is already present in Figure 5 (solid lines). Thus, a more realistic AN model, implemented in Earlab as described in the "Methods" section, was also used to test the effect of the background inhibition. The vector strength of the excitatory inputs derived from the Earlab AN model was close to 0.6 for low modulation frequencies (100–400 Hz) and gradually decreased to below 0.1 at high modulation frequencies (>1,000 Hz). The same set of parameters of the synaptic inputs was used and the generated rate–f_m functions were plotted as dashed lines in Figure 5. For both N_I=20 and 200, including the f_m-dependent synchronization in the AN inputs did not significantly alter the rate–f_m functions except that the rates at low modulation frequencies (100–300 Hz) were slightly increased for the case where the rate–f_m function showed a clear single peak. This rate

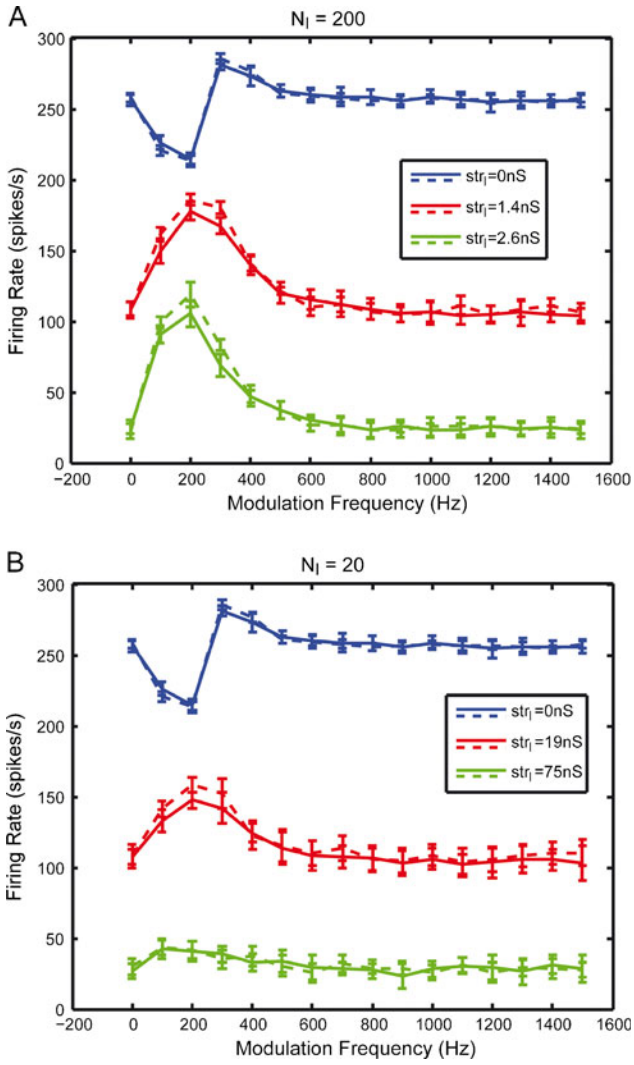

FIG. 5. Rate–f_m functions of the HH-type LSO model with inhibitory inputs. *Different colors* represent different levels of inhibition strength str_I. **A** Number of inhibitory inputs equals 20. **B** Number of inhibitory inputs equals 200. *Solid lines* represent responses with simplified AN inputs. *Dashed lines* represent responses with Earlab AN inputs (see "Results"). For all cases shown, $rate_{mean}$=200 spikes/s, str_E=2.55 nS, N_E=20, and $rate_I$=30 spikes/s.

increase might reflect the increased phase locking of the Earlab AN inputs at low modulation frequencies. The similarity between the rate–f_m functions with or without the envelope filtering in the input is presumably due to the low-pass filtering in the synapse and the cell membrane which restrict the frequency range for phase locking independent of the presence of the envelope filtering in the input.

We interpret the results shown in Figure 5 to indicate that the background inhibition alone can give rise to small rate decays (RPH around 50 spikes/s), but cannot fully explain large rate decays (RPH>100 spikes/s). In order to reproduce rate–f_m functions with RPH around 100 spikes/s, the background inhibition requires a low level of randomness even with inputs from the Earlab AN model that captures envelope filtering. This low level of randomness is only available with much larger number of the inhibitory inputs than the number estimated empirically (Sanes 1990). Lower values for the average excitatory input rate were also tested. When $rate_{mean}$ is equal to 100 spikes/s, the rate–f_m functions for both N_I=20 and N_I=200 were similarly flat with the amplitude of the rate decay less than 50 spikes/s (results not shown).

HH-type LSO model with the KLT channel

In this section, the behavior of the HH-type LSO model with KLT channels is studied with the inputs driven by either the simplified AN model or the Earlab AN model. No inhibitory input was included in this model. Results evaluating the effects of the KLT strength, the AN input rate, and the number of AN inputs show how these parameters influence the dependence of the rate of firing on the modulation frequency in this model.

Effect of the KLT strength on rate–f_m functions. To examine the effect of the KLT strength, the KLT conductance was varied while the number of excitatory inputs was set to 20 and the synaptic strength was fixed at 2.55 nS. Figure 6 shows the results for the simplified AN model with the $rate_{mean}$ parameter in Eq. 2 equal to 100 spikes/s. Three KLT conductance values were chosen (Fig. 6A) to illustrate the transition from an all-pass characteristic to a band-pass characteristic in the rate–f_m function. Without the KLT channel, the average rates of the LSO model response were above 100 spikes/s at all modulation frequencies and showed a small peak at 200 Hz. When the KLT channel conductance increased to 35 nS, the rates at high (above 800 Hz) modulation frequencies were reduced more than the rates at low f_m (say 200 Hz), which increased the RPH of the rate–f_m function. For even larger KLT conductance of 85 nS, the average rates of the response at high f_m became even lower while the rate at low f_m remained at a much higher level, further increasing the RPH to about 70 spikes/s. [When KLT channel conductances higher than 85 nS were tested in the model, the rate at low modulation frequencies remained low and the RPH became smaller (results not shown)]. Overall, the KLT channel strongly suppressed the responses at high modulation frequencies, contributing to the low-pass characteristic in the rate–f_m function, as shown in Figure 6A. This behavior is attributed to the suppressive effect of the KLT channel as documented by previous studies (Rothman and Manis 2003a, b, c). Another observation in Figure 6A is that the firing rate at 1,500 Hz approximately

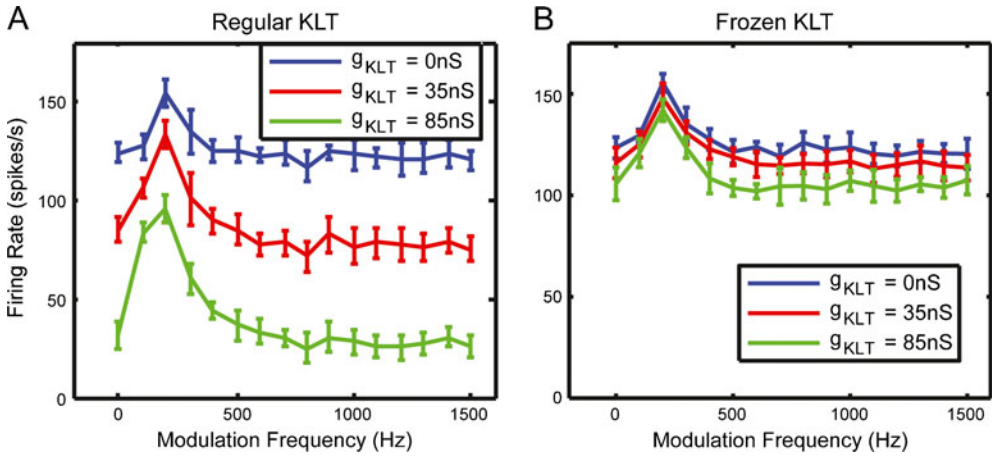

FIG. 6. **A** Rate–f_m functions of the HH-type LSO model with regular KLT channels. **B** Rate–f_m function of the LSO model with a "frozen KLT" channel. The "frozen KLT" channel was modeled as a leaky conductance that represented the KLT conductance at resting potential. For both **A** and **B**, $rate_{mean}$=100 spikes/s, str_E=2.55 nS, and N_E=20. The *blue*, *red*, and *green curves* correspond to g_{KLT} values of 0, 35, and 85 nS.

matched the firing rate at 0 Hz, independent of the absolute firing rate at 0 Hz. This characteristic was observed for all values of g_{KLT} tested and may be caused by the membrane filtering at high modulation frequencies.

The membrane time constant τ_m changed with g_{KLT} due to the influence of the KLT channel conductance on the total membrane conductance and thereby on τ_m (as discussed in the "Methods" section). To examine whether the emergence of the firing rate decay in the rate–f_m function (Fig. 6A) could be caused primarily by the change in τ_m, we used a "frozen KLT" model (Day et al. 2008). The KLT dynamics were removed in the model, causing the KLT current to essentially become another leak current. This frozen KLT model shared the same membrane conductance and τ_m as the regular KLT model when V_m was around the resting potential. As shown in Figure 6B, when the dynamical property of the KLT channel was eliminated, the rate–f_m functions with frozen KLT channels were similar to the rate–f_m function when no KLT was present (Fig. 6B, compare red and green curves to the blue curve). The firing rates at all modulation frequencies only slightly decreased as the "frozen KLT" conductance increased. This suggests that the rate decay produced by the LSO model with regular KLT channel is mainly caused by the dynamical characteristics of the KLT channel instead of the increase of the passive membrane conductance.

To review how KLT dynamics influence the rate–f_m function, we again compare three cases (no modulation, low f_m, and high f_m) as examples. In the case of no modulation (f_m=0 Hz), the input spikes can be considered as uniformly distributed in time, producing a relatively flat synaptic current with only small fluctuations. The KLT channel is opened shortly after the stimulus onset in the LSO cell model. Due to the constant synaptic stimulation, the KLT channel stays activated and effectively suppresses the ongoing spikes. At low (but non-zero) f_m, the synaptic current can be considered as a sinusoidal current injection with additive noise. In this case, the KLT channel is also opened shortly after the stimulus onset; however, since the period in the stimulus is relatively long, the membrane potential can return to resting potential in the interval between two adjacent peaks in the synaptic current ("off" duration). As a result, the KLT channel de-activates in "off" durations, and the cell can fire in response to most peaks in the stimulus, producing a higher firing rate. At high f_m, the membrane potential becomes relatively flat due to passive membrane filtering. In this case, the KLT channel stays activated after stimulus onset and blocks the ongoing spikes.

As in the case of the LSO model with inhibition, we also tested the LSO model with KLT channels using more realistic AN inputs. Figure 7 shows the simulation results for an average AN input rate $rate_{mean}$ equal to 200 spikes/s with two types of AN inputs. First, the simple AN model used to generate the results in Figure 6 was tested with a higher average rate (solid curves in Fig. 7A), and second, the Earlab AN model was used with the same higher average rate (dashed curves in Fig. 7A). Values for the KLT conductance parameter g_{KLT} were chosen as before: a value of zero and two additional values to give rates of 100 spikes/s and 25 spikes/s for the 1,500-Hz modulation frequency. In Figure 7A, note first that the rate–f_m functions with increasing g_{KLT} are qualitatively similar to those with $rate_{mean}$ equal to 100 spikes/s (Fig. 6A), although the maximum RPH with higher input rate in Figure 7A is around 160 spike/s, much higher than the maximum RPH with lower input rate (Fig. 6A). Second, the rate–f_m functions are similar with or without the f_m-dependent synchroni-

zation in the inputs (comparing dashed and solid curves). The Earlab AN inputs only slightly increased the peak rate of the rate–f_m functions (Fig. 7A, dashed lines). Therefore, the f_m-dependent synchronization in the AN inputs does not appear to be essential for creating the rate decay in the rate–f_m functions, but it may play a role in further increasing the RPH of the rate–f_m functions.

To confirm that the HH-type LSO model in the present study can also reproduce the tMTF of the LSO cells, the modulation gain of the LSO model was plotted as a function of f_m for different KLT strength (Fig. 7B, blue, red, and green curves). The modulation gain was computed as $20 \log(2R)$, where R is the synchronization index of the LSO response. The shape of these temporal MTFs exhibits the general low-pass characteristic seen in the LSO data (Joris and Yin 1998). The strength of the KLT channel did not significantly affect the shape of the tMTF. For more direct comparisons, the tMTF of the Earlab AN inputs is also shown in Figure 7B (solid black curve). It is clear that the maximum synchronization is enhanced in the responses of the LSO model relative to the Earlab AN inputs. Furthermore, the tMTFs of the LSO model show a more limited range of phase locking than the AN inputs (Fig. 7B, compare the 3-dB cutoff frequency of solid curves with that of the dashed black curve). The enhanced maximum synchronization and restricted frequency range exhibited in the LSO model are consistent with the LSO data measured empirically (Joris and Yin 1998). It is important to note that the transformations in the tMTF of the LSO described above were reproduced by the LSO model without KLT channels (Fig. 7B, blue curve). Therefore, the emergent features in the tMTF of the LSO must derive from mechanisms other than the KLT channel. Possible factors include dendritic filtering, smooth synaptic current due to convergent inputs from the CN, or the membrane filtering.

Effect of the input rate on rate–f_m functions. The results presented in the previous section show that the RPH of the rate–f_m functions not only depends on the KLT strength, but also on the input rate $\text{rate}_{\text{mean}}$ (compare Fig. 6A with 100 spikes/s to Fig. 7A with 200 spikes/s). In this section, the dependence of the response of a given LSO cell on stimulus level is characterized. Specifically, we examined the effects of the input rate on the rate–f_m function by varying the average rate for the excitation $\text{rate}_{\text{mean}}$. Similar to previous simulations, N_E was set to 20 and incre_E was set to 2.55 nS. Two fixed values for g_{KLT} were used when rate_E was varied. The LSO model with smaller KLT conductance (85 nS) shows tonic firing for large step currents while the LSO model with larger KLT conductance (160 nS) only exhibits up to three onset spikes for step currents with any amplitude that was tested (up to 2 nA).

For the smaller KLT conductance (85 nS), the response rate at all f_m increased as rate_E increased (Fig. 8A) and the RPH of the rate–f_m function changed little as the input rate increased. To examine the model responses to pure tones, the firing rate of the LSO model in response to pure tones was plotted as a function of the input rate (Fig. 8C) for the same parameter values used to generate the results in panel A. The simulated rate–level function is sigmoid-shaped with a maximum rate above 200 spikes/s, consistent with the features of the empirically measured rate–level functions in the LSO (Tsuchitani and Boudreau 1966; Boudreau and Tsuchitani 1970). When the KLT conductance became larger (160 nS), as the input rate was increasing, the rate at high f_m (>800 Hz) increased slightly while the rate at low f_m (100–500 Hz) significantly increased (Fig. 8B). As a result, the RPHs for large input rates (200 and 300 spikes/s) were much larger than that with small KLT conductance; however, for the larger g_{KLT}, the output rate in response to pure tones reached only about 60 spikes/s at the highest input rate tested (Fig. 8D). This suggests that the KLT current was so strong that even the strongest pure tone stimulus used was largely suppressed by the KLT channel. Consistent with the membrane filtering effect described previously in this paper, the output firing rate at high f_m mimicked the output firing rate without modulation, regardless of the KLT strength and the input rate (Fig. 8A,B).

To summarize, the present LSO model predicts that the effect of the input rate is dependent on the KLT conductance. A low KLT conductance combined with a low input rate can explain the rate decrease at high modulation frequencies without contradicting the measured high maximum firing rate to pure tones in the LSO (Tsuchitani and Boudreau 1966; Boudreau and Tsuchitani 1970). High KLT conductance could produce larger rate decrease in the rate–f_m function, while also greatly reducing the maximum firing rate in response to pure tones.

Effect of the number of inputs on rate–f_m functions. Based on the results presented in the previous two sections it appears that the KLT channel can largely explain the variability of the rate–f_m functions in the empirical LSO data; however, one issue of the LSO model with the KLT channel remains and is related to the SBCs in the AVCN. In spite of SBCs in adult guinea pigs being shown to contain KLT channels (Manis and Marx 1991; Rothman and Manis 2003a), the expected low-pass characteristic is not empirically observed in the rate–f_m functions of the SBCs. To the contrary, most of the rate–f_m functions in SBCs were relatively flat (Fig. 1A). One possible resolution to this difference may be the difference in the number of

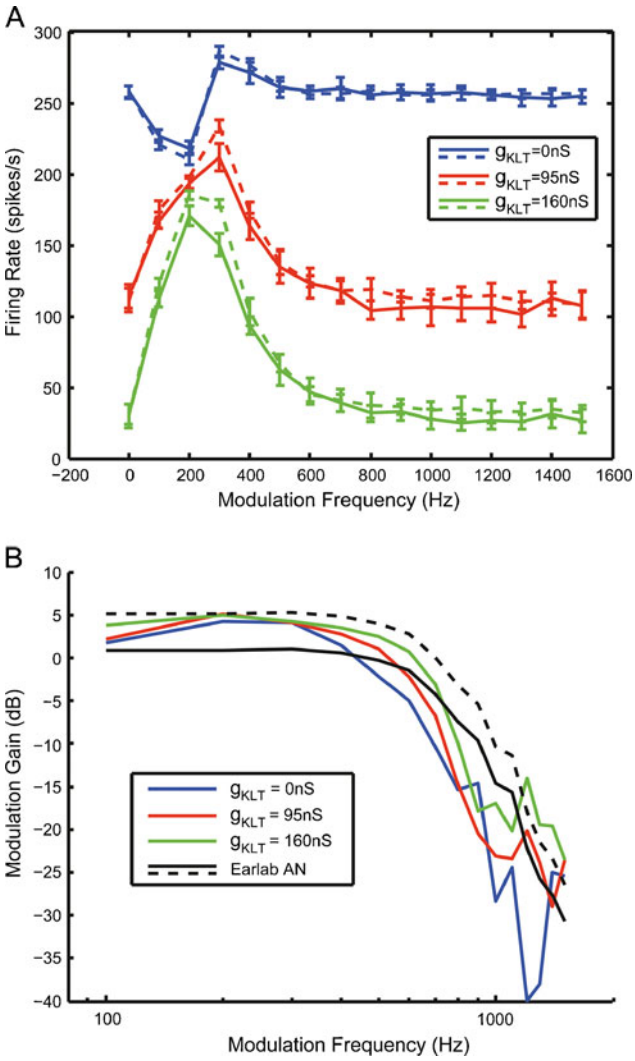

FIG. 7. **A** Rate–f_m functions with varying KLT conductance for the HH-type LSO model with regular KLT channels. *Different colors* represent different values of KLT strength g_{KLT}. *Solid lines* represent responses with inputs from the simplified AN model; *dashed lines* represent responses with inputs from the Earlab AN model (see "Results"). **B** tMTFs for the Earlab AN inputs and the HH-type LSO model with regular KLT channels. *Blue, red,* and *green curves* represent different KLT strength g_{KLT} as indicated. *Solid black curve* represents the tMTF for the Earlab AN inputs, and the *dashed black curve* is the same as the *solid black curve* except a constant vertical shift to emphasize the lower 3-dB cutoff frequency in the LSO model relative to the Earlab AN input. For all cases shown (**A** and **B**), $rate_{mean}$ is 200 spikes/s, str_E is 2.55 nS, and N_E is 20.

excitatory inputs received by SBC and LSO cells. The number of AN inputs to a single SBC in cats has been estimated to be around 1 to 4 (Ryugo and Sento 1991; Melcher 1993). In comparison, the estimated numbers of excitatory and inhibitory inputs to a single LSO cell were both around ten (Sanes 1990). It is possible that the effect of the KLT channel is affected by the number of excitatory inputs. In this section, we present the results of the KLT model with varying N_E. To eliminate any effect from changing the overall level of the excitation, the total amount of the excitatory conductance was fixed. In this case, changing the number of inputs affected only the temporal distribution of the excitatory conductance. Larger numbers of inputs reduced the effect of the random timing of each input spike, producing a smoother synaptic current that resembled the rate function of the underlying Poisson process. Specifically, the input rate was set to 100 spikes/s and the total amount of the excitatory conductance was fixed at 5.1 μS (equivalent to 20 inputs, with each input having a rate of 100 spikes/s and a synaptic strength of 2.55 nS).

As shown in Figure 9A, increasing the number of inputs while holding the KLT conductance g_{KLT} constant at 85 nS converted the rate–f_m function from all-pass to band-pass. At low input numbers, say N_E=2 as shown, the effect of the modulation frequency f_m of the inputs was obscured by the random timing of the input spikes. Thus, for small N_E, the LSO model cannot distinguish between inputs with different f_m and the output rate did not show a dependence on f_m for small N_E. As N_E increased, the randomness in the synaptic current was increasingly reduced by a larger number of input spikes. The LSO model was then able to detect the difference in the synaptic input, producing f_m-dependent rate functions.

Another way to view the effect of increasing input number is shown in Figure 9B, where the KLT conductance g_{KLT} was varied, as N_E increased, to produce a fixed firing rate (around 25 spikes/s) at 1,500 Hz modulation frequency. In this case, increasing N_E generated higher peak rates at low f_m when the rates at high f_m were fixed. In other words, the RPH of the rate–f_m function increased with increasing N_E. This could be understood with similar mechanisms as involved in Figure 9A. As N_E increased (e.g., 200), the synaptic current would become increasingly similar to the rate function of the underlying Poisson process with less noise. Therefore, at low f_m, the membrane potential could reliably exceed the firing threshold in a larger number of modulation cycles, thus giving rise to a higher firing rate. Another observation in Figure 9B is that smaller g_{KLT} values are required to maintain a low firing rate at 1,500 Hz for a larger number of inputs. This is because the KLT channel suppressed spikes more effectively with a stable synaptic current than with a fluctuating synaptic current. As N_E increased, the fluctuation in the synaptic current at high f_m was reduced, which increased the effectiveness of the KLT channel. Therefore, to obtain the same firing rate at high f_m, lower KLT conductance was required with larger N_E.

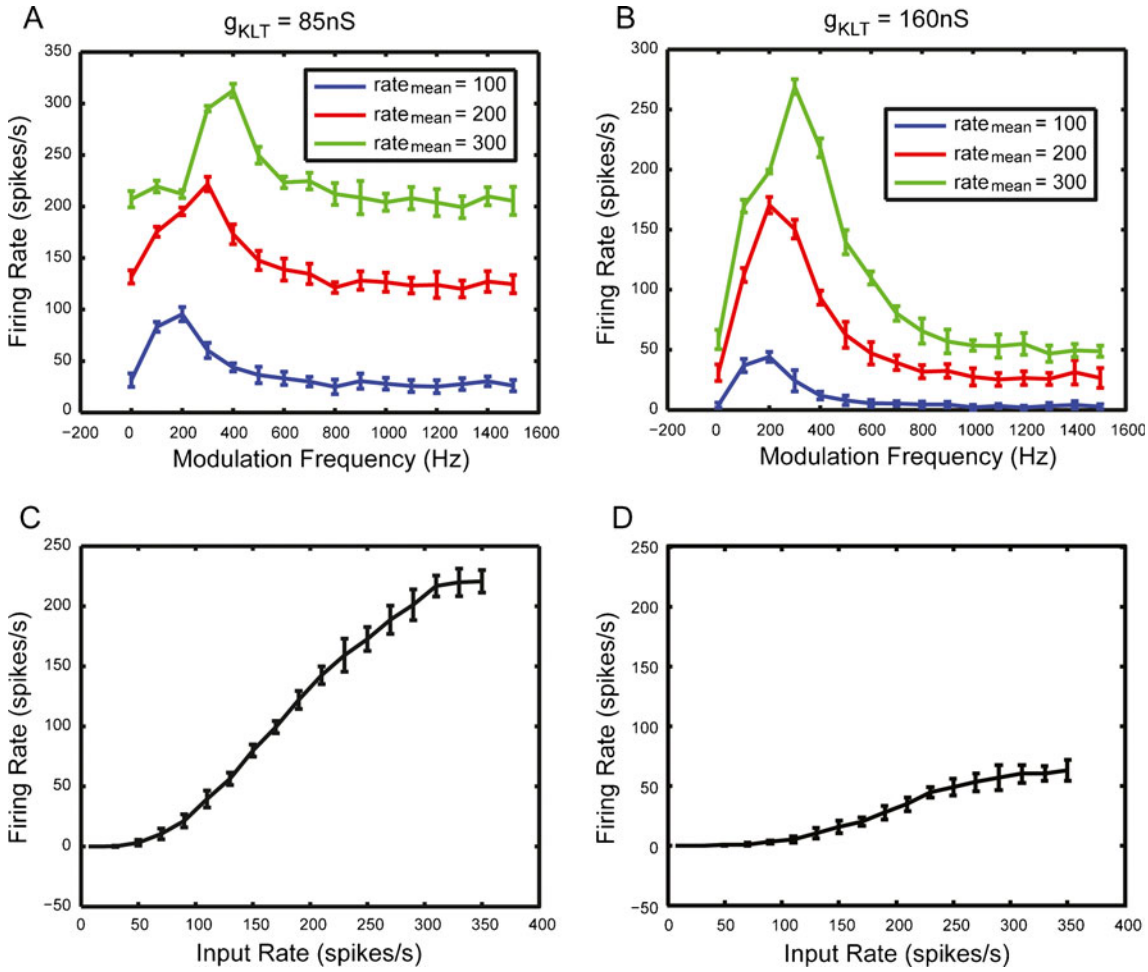

FIG. 8. **A**, **B** Rate–f_m functions with varying excitatory input rate for the HH-type LSO model with regular KLT channels. *Different colors* represent different values of input rate. **C**, **D** Response rate of the LSO model as a function of the input rate $rate_{mean}$ with unmodulated inputs. The KLT channel conductance g_{KLT} was 85 nS for **A** and **C** and 160 nS for **B** and **D**. For all panels, str_E=2.55 nS and N_E=20.

The results in Figure 9A suggest that very low input numbers could give rise to a flat rate–f_m function, which could potentially explain the flat rate–f_m function in the SBC. However, this explanation was based on the results from an LSO cell model instead of an SBC model. To test the explanation more rigorously, we took the same SBC model as in Rothman and Manis (2003c) with exactly the same parameters they used in their paper. The input number was set to two and the input rate was fixed at 200 spikes/s. As synaptic strength str_E increased, the overall rate also increased (Fig. 9C). The shape of the rate–f_m functions was consistently flat, independent of the value for str_E. This result suggests that the difference in the input number of the LSO and the SBC is very likely to play a role in creating different shapes of the rate–f_m functions in response to SAM tones.

LSO responses to contralateral modulation. In addition to LSO responses to ipsilateral SAM tones, LSO responses to contralateral modulation were also measured in Joris and Yin (1998) by stimulating the ipsilateral ear with an unmodulated tone while presenting a SAM tone contralaterally. Compared with the rate decrease with ipsilateral modulation (Fig. 1B), the firing rate of LSO cells in response to contralateral modulation showed a similar but less variable decrease as modulation frequency increased (Fig. 1C). Joris and Yin (1998) suggested that the rate decrease for contralateral modulation was due to the loss of envelope phase locking at high modulation frequencies because a sustained MNTB input at high f_m inhibits the LSO cell more effectively than a modulated MNTB input at low f_m. The HH-type LSO developed in the present study was used to reproduce the firing rate as a function of the modulation frequency for contralateral modulation. In this simulation, the input model was the same Earlab AN model described previously except that the stimulus was a pure tone for the ipsilateral ear and a SAM tone for the contralateral ear. Preliminary simulation results showed that the HH-type LSO model was capable of reproducing the rate decrease for

contralateral modulation when no KLT channel was present. Increasing the KLT conductance reduced the firing rate at all modulation frequencies and did not further increase the amplitude of the rate decrease. These results are consistent with the explanation for this rate decrease suggested by Joris and Yin (1998) and indicate a minor role for the KLT channel in the firing rate decrease in response to contralateral modulation.

DISCUSSION

Computational modeling of LSO neurons was used to explore several hypotheses to explain the dependence of neural firing rate on modulation frequency as observed in the LSO responses to SAM tones. The main findings of this study are:

1. The presence of KLT channels, combined with the passive membrane filter in the LSO, could largely account for the observed dependence of rate on the modulation frequency in the LSO responses to ipsilateral SAM tones. The same LSO model could also reproduce the enhanced maximum synchronization and the more limited frequency range for phase locking in the tMTFs of the LSO relative to the SBC inputs.
2. The model with AHP channels, which were compatible with those incorporated in previous LSO models, showed the expected effects on sequential dependence of firing times, but these channels made minimal contribution to the firing rate decrease in LSO responses to ipsilateral modulation. Thus, the AHP channels, although important for some temporal behavior, are unlikely to be the primary factor underlying the rate decay at high modulation frequencies.
3. Background inhibition, possibly generated from the spontaneous activity of the MNTB, could give rise to small rate decreases at high modulation frequency; however, due to the realistic fluctuations, as expected for the empirically estimated number of inputs, the level of inhibition is not sufficiently steady to generate large rate decreases at high modulation frequency. The required regularity could be achieved but with much larger numbers of inputs than estimated empirically. Thus, the background inhibition hypothesis appears to be a plausible explanation for the low-pass-shaped rate–f_m functions with small rate decrease and is not sufficient to account for the rate–f_m functions with a large rate decrease.
4. The rate decrease with modulation frequency in the LSO responses to contralateral modulation could be explained by the loss of the phase locking in the inhibitory inputs at high modulation frequencies. The KLT channel does not appear to be an important factor in generating the rate decrease in response to contralateral modulation.

In the rest of this section, we discuss several issues that arise when the KLT channels are assumed to be the primary mechanism for the observed dependence of rate on modulation frequency in responses to ipsilateral SAM tones. These issues include the observed density of KLT channels in LSO neurons, the relationship between the rate with no modulation (f_m=0) and the rate at high modulation frequency, the dependence of firing rate on input level for different modulation frequencies, and some aspects of available data that are difficult to understand with the KLT hypothesis. Finally, this section ends with comparisons of the effects of the multiple channel types that are believed to be present in the LSO cell membrane and of the differences between responses of neurons in various brainstem nuclei with similar channels.

Presence of KLT channels in the LSO

While slice data of the LSO in cat are scarce, several studies have sought to examine the intrinsic properties of the LSO cells in rodents. One of these studies argued that the density of the KLT channel in the LSO decreases in the lateral to medial direction (Barnes-Davies et al. 2004). The characteristic frequency of the LSO cells in Figure 1B ranges from 5 to 30 kHz, roughly mapping to the central one third of the LSO in cat (Tsuchitani and Boudreau 1966; Joris and Yin 1998). If we assume that the LSO in cat has a KLT channel density gradient similar to that seen in rat (an assumption that needs to be tested with more data in cat), then it is possible that the LSO cells in Figure 1B contain a significant number of KLT channels. As described previously in this paper, a relatively small amount of KLT conductance in the model may be sufficient to induce the firing rate decay in the rate–f_m function, especially for a large number of inputs (Figs. 8A, C and 9B). Furthermore, based on the modeling result with varying KLT strength (Figs. 6A and 7A), it can be speculated that the variability of the rate at the highest modulation frequency (Fig. 1B) is related to the variability of the KLT density in those LSO cells.

Band-pass vs. low-pass f_m dependence

A general observation of the modeling results in the present study is that the response rate with no modulation (f_m=0 Hz) matches the rate at highest f_m (1,500 Hz), regardless of the absolute rate value at the highest f_m. This may appear surprising at first but is consistent with the notion that effective synaptic

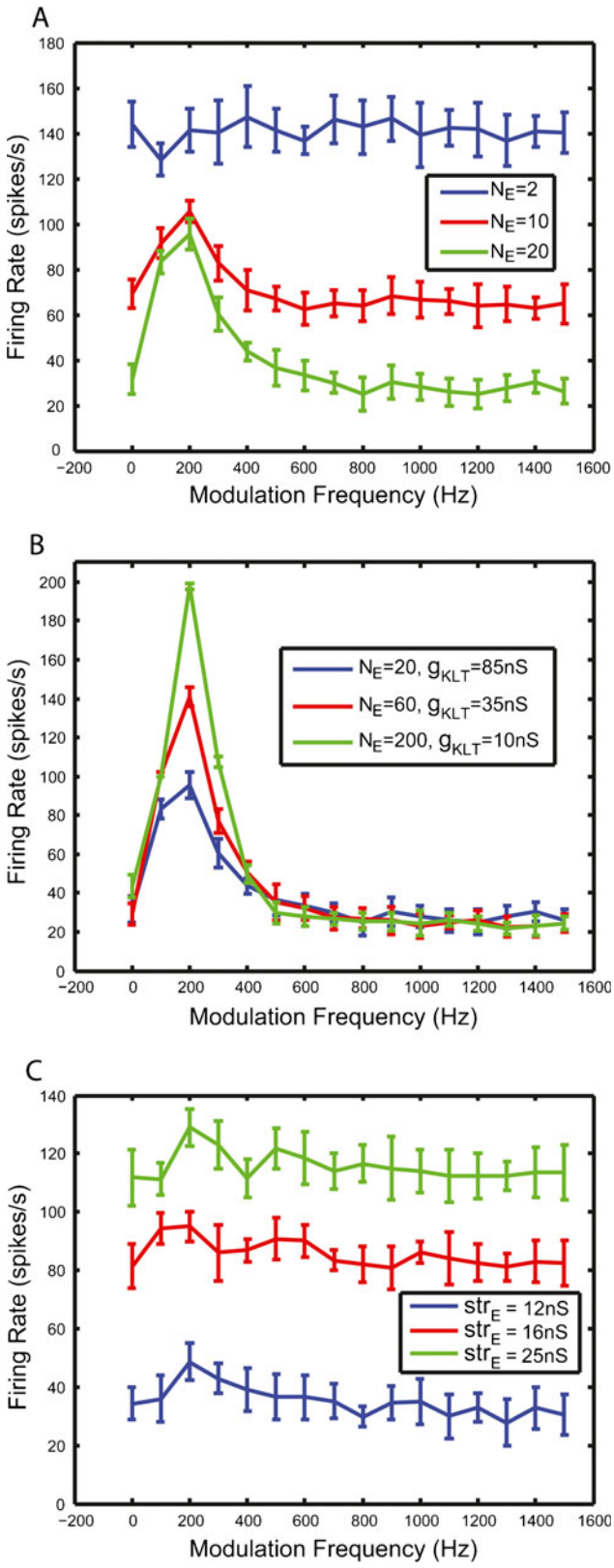

FIG. 9. **A** Rate–f_m functions with varying input number while fixing the total amount of excitatory conductance and the KLT strength for the HH-type LSO model. *Different colors* represent different numbers of excitatory inputs. For these cases, total_str$_E$=5.1 μS, g_{KLT}=85 nS, and rate$_{mean}$=100 spikes/s. **B** Rate–f_m functions with varying input number while fixing the total amount of excitatory conductance and the firing rate at 1,500 Hz for the HH-type LSO model. *Different colors* represent different numbers of excitatory inputs and corresponding KLT strength. For these cases, total_str$_E$=5.1 μS and rate$_{mean}$=100 spikes/s. **C** Rate–f_m functions with varying excitatory synaptic strength str$_E$ for the SBC model. *Different colors* represent different values of excitatory synaptic strength str$_E$. For these cases, rate$_{mean}$=200 spikes/s, N_E=2, and g_{KLT}=200 nS.

inputs at 0 and 1,500 Hz are similar due to the passive membrane filtering at high frequency (1,500 Hz). Therefore, to reproduce the observed low-pass feature (i.e., negative slope) at high modulation frequencies (say above 400 Hz), the model necessarily also predicts a positive (high-pass) slope at low modulation frequencies (from 0 to 200 Hz). Unfortunately, there are no data to test this hypothesis. The rate in response to pure tones was not systematically measured in Joris and Yin (1998) at the sound level they used to measure SAM tone responses. While LSO data that directly test this model prediction are not available, the characterizations of the response properties of a few LSO units in Joris and Yin (1998) are in partial agreement with this prediction. Their rate–f_m functions increased with f_m at low modulation frequencies, as expected from the model. Furthermore, previous studies have shown that phasic firing neurons (in response to steady current input) respond poorly to low-frequency sinusoidal current injection (Beraneck et al. 2007; Gai et al. 2010). Therefore, these neurons exhibit a band-pass characteristic in their rate–input frequency function. This is consistent with the results in the present study that show band-pass-shaped rate–f_m functions with low firing rate at zero frequency.

From a physiological point of view, the firing rates of the LSO at 0 and 1,500 Hz are expected to be similar if the inputs to the LSO are SBC-like. In actual SBC responses to SAM tones, there is little change in the average rate with increasing f_m (Joris and Yin 1992, 1998), and the vector strength decreases as the modulation frequency increases (Frisina et al. 1990a; Joris and Yin 1998; Rhode and Greenberg 1994). Typically, the phase locking to the envelope becomes very weak at very high f_m (above 1,500 Hz) for the SBC. Therefore, the responses of the SBC at 0 and 1,500 Hz share similar rates and both lack temporal structures caused by phase locking to the envelope. If the inputs to the LSO are SBC-like (as in the present model), it would be very unlikely that the LSO cell can distinguish the inputs at 0 and 1,500 Hz and produces different rates. In fact, it would be an important observation if a future empirical study were to show a large difference in LSO firing rates at 0 and 1,500 Hz when the inputs have the same sound level because that would suggest that either the inputs at 0

and 1,500 Hz are not very similar, or some more complicated mechanisms in the LSO cell may allow for very similar input spike patterns to be distinguished.

The above analysis is complicated by the observation that many of the excitatory projections to high-frequency LSO cells originate from ipsilateral small spherical bushy cells (Cant and Casseday 1986). Unfortunately, the cellular properties and the synaptic inputs of these small bushy cells are not well characterized. In any case, the present study is based on the assumption that the inputs to the LSO cell are similar to the AN responses, consistent with previous modeling studies on the LSO (Zacksenhouse et al. 1998; Zhou and Colburn 2010).

Response rate to pure tones

Previous in vivo studies in the LSO have shown that LSO cells can respond at relatively high rates to pure tones (Tsuchitani and Boudreau 1966; Tsuchitani 1988a, b). In contrast, the model in the present paper predicted low response rates for pure tones in these experiments being modeled in order to reproduce low rates at the highest f_m in the empirical data (Fig. 1B). However, the low rate prediction of the model does not necessarily contradict the measured high rate in response to pure tones. In the primary study modeled here (Joris and Yin 1998), sound levels were chosen to maximize the synchrony of the LSO responses to the envelopes of the SAM tones at 100 Hz. The maximum synchronization tends to occur between the threshold and the maximum firing rate for the AN (Joris and Yin 1992; Dreyer and Delgutte 2006) and for the CN (Frisina et al. 1990a). Therefore, the sound level used by Joris and Yin (1998) is expected to be significantly lower than that which maximally drives the LSO cell. The relatively low input level may account for the low rate at 0 Hz in some of the model predictions. This hypothesis is consistent with the model result with varying input rates (Fig. 8). The results in Figure 8A and C suggest that the LSO cells with small KLT conductance can both respond well to pure tones at high levels and also produce band-pass-shaped rate–f_m functions at low levels.

This prediction that cells with KLT channels could respond well to pure tones is consistent with the SBC data. For example, it was shown that the large SBC in mammalian brainstem contains a KLT conductance that is strong enough to make the SBC an onset cell in response to current steps (Rothman and Manis 2003a). On the other hand, the firing rate of the primary-like units (likely SBCs) can be well above 200 spikes/s at high input levels in response to pure tones (Bourk 1976; Frisina et al. 1990b). Nevertheless, if the KLT conductance is too strong, then the cell will not be able to achieve high rates to pure tones (Fig. 8B, D). This appears to be an area in which further experiments would be useful.

Limitations of the LSO model with KLT channels

Even though the LSO model that includes KLT channels can reproduce most of the variability in the empirically measured rate–f_m functions, it also has some limitations. The first one is the low peak rate that is observed when the rate–f_m function is simulated with a low input rate (Fig. 6A, green curve). In comparison with the empirical data, for the LSO cell with very low rate at the highest f_m, the peak rates are usually above 100 spikes/s (Fig. 1B). Increasing the input rate and KLT conductance in the model enhanced the amplitude of the rate decrease without affecting the rate at the highest f_m (Fig. 7A, solid green line); however, higher input rate for single fibers (200 spikes/s in Fig. 7) may not be consistent with the measured rate in SBCs (Fig. 1A). Furthermore, higher KLT conductance leads to low excitability to pure tones (Fig. 8D). Another way to increase the peak rate is to use a higher number of inputs while fixing the total amount of excitatory conductance (Fig. 9B). The benefit of using a larger number of inputs is that the KLT conductance required to reduce the firing rate at 1,500 Hz to below 50 spikes/s becomes lower. With low KLT conductance, the LSO model can respond very well to pure tone stimuli at high input levels.

Very few studies have tried to estimate the number of inputs to the LSO. The only estimate that the authors are aware of was presented in Sanes (1990). The estimated number of inputs for the excitation and inhibition were both around ten. This estimation was based on brainstem slice data, which implies some of the inputs may be left out in the estimation. Therefore, their estimation should be interpreted as a lower bound for the actual input number. Based on Sanes (1990), we chose 20 as the default input number in this study. Nonetheless, more data are required to determine if using a high number of inputs are realistic.

The second drawback is the lack of variability in the cutoff frequency in the simulated rate–f_m functions. The LSO model with KLT channels in the present paper consistently shows peaks around 200 Hz in the rate–f_m function and the firing rate decrease tends to finish before f_m reached 500 Hz. In contrast, empirical rate–f_m functions show a wider range of the cutoff frequency. For example, a few LSO cells (Fig. 1B) maintained a high firing rate for f_m up to around 500 Hz. Preliminary modeling results suggest that

changes in the membrane time constant and the synaptic time constant in the LSO model are not sufficient to reproduce the wide range of the cutoff frequencies in the empirical rate–f_m functions. More simulations are needed to determine the parameter set that could fully account for the variability of the cutoff frequency in the empirical data.

The third drawback is that the LSO model in the present study cannot reproduce all of the rate–f_m functions in Figure 1B. In particular, two LSO units (solid diamond and solid square in Fig. 1B) showed an unusual combination of three features in their rate–f_m functions: (1) a very high firing rate (>200 spike/s) at the lowest f_m measured (50 or 100 Hz); (2) a monotonic decrease in the firing rate as the f_m increased; and (3) a low firing rate (<50 spikes/s) at the highest f_m measured. A closer look at those two rate–f_m functions reveals 2 to 4 spikes/cycle at frequencies of 50 to 100 Hz and that the spikes/cycle drops to below 1 spike/cycle at 200 Hz. For all the parameter sets that were used, the LSO model in the present study was unable to capture all three features of the rate–f_m functions at the same time. When the model cell reproduced the high spike count per cycle at low f_m (below 100 Hz), it also predicted an increasing firing rate as f_m increased from 100 to 300 Hz, different from the monotonic decrease in the firing rate in those two units. When the model cell exhibited a monotonically decreasing firing rate as the modulation frequency increased from 50 Hz, the response rate at the lowest f_m (50 Hz) was much smaller (around 50 spikes/s) than the firing rate in the data. Based on these unsuccessful simulation attempts, some speculations could be made for this monotonic rate decay with an RPH greater than 200 spikes/s observed in those two cells. One hypothesis is that these rate–f_m functions may be truly low-pass (high firing rate at zero frequency). If this is true, one possibility is that the input rate at 0 Hz modulation is significantly higher than the input rate with a modulation frequency of 1,000 Hz, suggesting that the inputs to those two LSO units are not SBC-like. Another possibility is that additional synaptic inputs may be involved in those two LSO units (e.g., ipsilaterally driven inhibition) to create different firing rates for 0 and 1,500 Hz modulation frequencies. On the other hand, if the rate of response to pure tones is low for those two LSO units (band-pass rate–f_m functions), then other factors such as the synapse location and dendritic filtering may play a role in producing the steep positive slope (high-pass) between zero frequency and the lowest f_m measured in those two LSO units.

Different rate–f_m functions for the SBC and the LSO cell

Another point to discuss is the observed difference in response patterns of cells in the LSO relative to the SBCs when KLT channels are present in both cell types. It is shown that the effect of the KLT channel on generating the rate decrease in the rate–f_m function is dependent on the number of inputs (Fig. 9). Thus, by using a small number of inputs to the SBC, the model successfully reproduced the flat rate–f_m functions observed in the SBC (Figs. 1A and 9C). This result is consistent with the supposition that, with a low number of inputs and strong synaptic connection strengths, SBCs largely function as a relay that faithfully recreates the activity from the AN input. This notion is supported by the empirical studies which showed that the responses of SBCs to SAM tones were very similar to those of the AN in terms of the flat rate–f_m function, maximum synchronization index, and cutoff frequency in the tMTF (Frisina et al. 1990a; Joris and Yin 1992; Rhode and Greenberg 1994). On the other hand, the larger number of converging inputs on the LSO cell, along with weaker synaptic connection strength, gives rise to stronger synaptic summation and smoother overall synaptic currents that better represent the envelope of the acoustic stimulus. The membrane filter, together with the firing threshold nonlinearity, then transforms the smooth synaptic inputs to f_m-dependent firing rates. In addition, the enhanced phase locking to the stimulus envelope in the LSO relative to the SBC may also be attributed to the smoother synaptic currents in the LSO.

AHP channels

As previously noted, the temporal aspects of LSO response to tone bursts, notably the level-dependent interval statistics, can be largely accounted for by the membrane AHP channels (Zhou and Colburn 2010). Even though the LSO model with KLT channels is capable of explaining neural responses to SAM tones, it is not expected to explain the temporal aspects of the LSO responses to tone bursts. This is because the KLT channels used in the present study are fundamentally different from the AHP channels in the Zhou and Colburn (2010) model. The KLT channel is activated if the membrane potential is above the KLT activation threshold (roughly −60 mV). The time course of the KLT conductance is simply a filtered and rectified version of the membrane potential. Due to the fast activation and decay of the KLT channels, the KLT conductance at each time point only reflects the recent history (less than 5 ms) of the membrane potential. This short-time information is a poor

representation of the firing history since it is not only very limited in time but also affected by the subthreshold membrane depolarizations. Thus, the KLT channels are not expected to determine the spike interval statistics in the LSO responses to tone bursts. On the other hand, the AHP conductance only depends on the firing activity of the model cell. The LSO model in Zhou and Colburn (2010) is not capable of reproducing the neural responses to SAM tones because the AHP channels cannot stay in an activated state to suppress firing activity when only subthreshold activity is present. To summarize, the AHP channels and the KLT channels appear to function independently in determining different aspects of the LSO responses. Both channels are needed to reproduce the LSO data with tone bursts and SAM tones with one comprehensive LSO model.

Possible roles of I_A and I_h currents

This study focused on the effect of the KLT channel. The reason for this is that we think the KLT channels are most relevant to the data we were trying to reproduce, and we think a parsimonious model provides cleaner interpretations of the effect of each model parameter. Besides the KLT channel, the A-type potassium channel (I_A) and the hyperpolarization-activated channel (I_h), both believed to be present in the LSO (Adam et al. 2001; Leao et al. 2006), are also considered in the context of the data in Figure 1B. The A-current I_A is a transient current that is activated by supra-threshold depolarization, and it lasts for tens of milliseconds (Rothman and Manis 2003b). The dynamics of this channel is similar to that of the AHP channel in the LIF model. As shown in the "Results" section, the AHP channel alone is unlikely to create the low-pass-shaped rate–f_m function, which suggests that I_A is unlikely to be an important contributor either. The I_h current by itself is also unlikely to produce the f_m dependence in the firing rate. Although it is conceivable that if the I_h channel is slightly opened at the resting potential and is inactivated by the depolarization caused by input EPSCs, the overall result would be a decrease in the depolarizing current, which has effects that are similar to an increase in the repolarizing current (such as the KLT current); however, due to the small amount of the I_h current at resting potential, the repolarizing current generated by inactivating the I_h is expected to be much smaller than that generated by activating the KLT channels. In addition, the inactivation of I_h channels is very slow (above 200 ms at the resting potential), which limits its ability to follow the modulation in the stimulus even for f_m as low as 50 Hz. Thus, the I_h is unlikely to create the low-pass-shaped rate–f_m function by itself. Though unlikely to be the primary mechanisms underlying the rate-tuning for the modulation frequency, the I_A and I_h channels may play roles in refining the prediction of the KLT model.

CONCLUSION

Overall, the modeling study presented here suggests that KLT channels can largely explain the low-pass-shaped rate–f_m function observed empirically in the LSO, while arguing that the AHP channel is not the main underlying mechanism. Furthermore, the background inhibition may play the major role in small rate decreases (Fig. 5A, red line); however, when the input number is physiologically realistic, the LSO model with inhibition failed to reproduce large rate decreases seen in some LSO units. Based on the simulation results for the LSO model with KLT channels, the stimulus level and the number of inputs are important factors in determining the shape of the rate–f_m function. Experiments measuring the complete rate–f_m function (particularly including 0 Hz modulation) in the LSO at increasing sound levels would be able to verify or contradict the model prediction about the firing rate at 0 Hz and the effect of the input level. Other mechanisms can also contribute to the rate dependence on the modulation and future experiments will help distinguish between different possible mechanisms.

We emphasize that it is not our intention to conclude that the KLT channel and the background inhibition are mutually exclusive. Simulation results of the present LSO model suggest that adding inhibition to the LSO model with KLT channels does not change the important features in the tMTF. In addition, the amplitude of the rate decrease produced by the combination of the KLT channel and the background inhibition lies in between the rate decreases generated by the KLT channel and the inhibition individually, given that the excitatory inputs and the firing rate at the highest f_m are held unchanged (results not shown). These results suggest that it is possible that both of them are present in LSO cells and work together to produce the rate decrease in the rate–f_m functions.

ACKNOWLEDGMENTS

This work was supported by NIH-NIDCD DC00100. We thank three anonymous reviewers for many useful suggestions.

OPEN ACCESS

REFERENCES

Adam TJ, Finlayson PG, Schwarz DW (2001) Membrane properties of principal neurons of the lateral superior olive. J Neurophysiol 86:922–934

Barnes-Davies M, Barker MC, Osmani F, Forsythe ID (2004) Kv1 currents mediate a gradient of principal neuron excitability across the tonotopic axis in the rat lateral superior olive. Eur J Neurosci 19:325–333

Batra R, Kuwada S, Fitzpatrick DC (1997) Sensitivity to interaural temporal disparities of low- and high-frequency neurons in the superior olivary complex. I. Heterogeneity of responses. J Neurophysiol 78:1222–1236

Beraneck M, Pfanzelt S, Vassias I, Rohregger M, Vibert N, Vidal PP, Moore LE, Straka H (2007) Differential intrinsic response dynamics determine synaptic signal processing in frog vestibular neurons. J Neurosci 27:4283–4296

Blum JJ, Reed MC (1991) Further studies of a model for azimuthal encoding: lateral superior olive neuron response curves and developmental processes. J Acoust Soc Am 90:1968–1978

Boudreau JC, Tsuchitani C (1968) Binaural interaction in the cat superior olive S segment. J Neurophysiol 31:442–454

Boudreau JC, Tsuchitani C (1970) Cat superior olive S-segment cell discharge to tonal stimulation. Contrib Sens Physiol 4:143–213

Bourk TR (1976) Electrical response of neural units in the anteroventral cochlear nucleus of the cat. PhD Dissertation, MIT, Cambridge

Cant NB, Casseday JH (1986) Projections from the anteroventral cochlear nucleus to the lateral and medial superior olivary nuclei. J Comp Neurol 247:457–476

Carney LH (1993) A model for the responses of low-frequency auditory-nerve fibers in cat. J Acoust Soc Am 93:401–417

Colburn HS, Moss PJ (1981) Projections to the lateral and medial superior olivary nuclei from the spherical and globular bushy cells of the anteroventral cochlear nucleus. In: Syka J, Aitkin L (eds) Neuronal mechanisms of hearing. Plenum, New York, pp 283–288

Day ML, Doiron B, Rinzel J (2008) Subthreshold K+channel dynamics interact with stimulus spectrum to influence temporal coding in an auditory brain stem model. J Neurophysiol 99:534–544

Dreyer A, Delgutte B (2006) Phase locking of auditory-nerve fibers to the envelopes of high-frequency sounds: implications for sound localization. J Neurophysiol 96:2327–2341

Finlayson PG, Caspary DM (1991) Low-frequency neurons in the lateral superior olive exhibit phase-sensitive binaural inhibition. J Neurophysiol 65:598–605

Frisina RD, Smith RL, Chamberlain SC (1990a) Encoding of amplitude modulation in the gerbil cochlear nucleus: I. A hierarchy of enhancement. Hear Res 44:99–122

Frisina RD, Smith RL, Chamberlain SC (1990b) Encoding of amplitude modulation in the gerbil cochlear nucleus: II. Possible neural mechanisms. Hear Res 44:123–141

Gai Y, Doiron B, Rinzel J (2010) Slope-based stochastic resonance: how noise enables phasic neurons to encode slow signals. PLoS Comput Biol 6:e1000825

Goldberg JM, Brown PB (1969) Response of binaural neurons of dog superior olivary complex to dichotic tonal stimuli: some physiological mechanisms of sound localization. J Neurophysiol 32:613–636

Hewitt MJ, Meddis R (1994) A computer model of amplitude-modulation sensitivity of single units in the inferior colliculus. J Acoust Soc Am 95:2145–2159

Hines ML, Carnevale NT (1997) The NEURON simulation environment. Neural Comput 9:1179–1209

Johnson DH, Dabak A, Tsuchitani C (1990) Function-based modeling of binaural processing: interaural level. Hear Res 49:301–319

Joris PX (1996) Envelope coding in the lateral superior olive. II. Characteristic delays and comparison with responses in the medial superior olive. J Neurophysiol 76:2137–2156

Joris PX, Yin TC (1992) Responses to amplitude-modulated tones in the auditory nerve of the cat. J Acoust Soc Am 91:215–232

Joris PX, Yin TC (1995) Envelope coding in the lateral superior olive. I. Sensitivity to interaural time differences. J Neurophysiol 73:1043–1062

Joris PX, Yin TC (1998) Envelope coding in the lateral superior olive. III. Comparison with afferent pathways. J Neurophysiol 79:253–269

Leao KE, Leao RN, Sun H, Fyffe RE, Walmsley B (2006) Hyperpolarization-activated currents are differentially expressed in mice brainstem auditory nuclei. J Physiol 576:849–864

Lopez-Poveda EA, Meddis R (2001) A human nonlinear cochlear filterbank. J Acoust Soc Am 110:3107–3118

Manis PB, Marx SO (1991) Outward currents in isolated ventral cochlear nucleus neurons. J Neurosci 11:2865–2880

Melcher JR (1993) The cellular generators of the brainstem auditory evoked potential. PhD Dissertation, MIT, Cambridge

Mountain DC, Cody AR (1999) Multiple modes of inner hair cell stimulation. Hear Res 132:1–14

Nelson PC, Carney LH (2004) A phenomenological model of peripheral and central neural responses to amplitude-modulated tones. J Acoust Soc Am 116:2173–2186

Reed MC, Blum JJ (1990) A model for the computation and encoding of azimuthal information by the lateral superior olive. J Acoust Soc Am 88:1442–1453

Rhode WS, Greenberg S (1994) Encoding of amplitude modulation in the cochlear nucleus of the cat. J Neurophysiol 71:1797–1825

Rothman JS, Manis PB (2003a) Differential expression of three distinct potassium currents in the ventral cochlear nucleus. J Neurophysiol 89:3070–3082

Rothman JS, Manis PB (2003b) Kinetic analyses of three distinct potassium conductances in ventral cochlear nucleus neurons. J Neurophysiol 89:3083–3096

Rothman JS, Manis PB (2003c) The roles potassium currents play in regulating the electrical activity of ventral cochlear nucleus neurons. J Neurophysiol 89:3097–3113

Ryugo DK, Sento S (1991) Synaptic connections of the auditory nerve in cats: relationship between endbulbs of held and spherical bushy cells. J Comp Neurol 305:35–48

Sanes DH (1990) An in vitro analysis of sound localization mechanisms in the gerbil lateral superior olive. J Neurosci 10:3494–3506

Smith PH, Joris PX, Yin TC (1993) Projections of physiologically characterized spherical bushy cell axons from the cochlear nucleus of the cat: evidence for delay lines to the medial superior olive. J Comp Neurol 331:245–260

Smith PH, Joris PX, Yin TC (1998) Anatomy and physiology of principal cells of the medial nucleus of the trapezoid body (MNTB) of the cat. J Neurophysiol 79:3127–3142

Smith PH, Joris PX, Carney LH, Yin TC (1991) Projections of physiologically characterized globular bushy cell axons from the cochlear nucleus of the cat. J Comp Neurol 304:387–407

Tollin DJ, Yin TC (2005) Interaural phase and level difference sensitivity in low-frequency neurons in the lateral superior olive. J Neurosci 25:10648–10657

Tsuchitani C (1988a) The inhibition of cat lateral superior olive unit excitatory responses to binaural tone bursts. II. The sustained discharges. J Neurophysiol 59:184–211

Tsuchitani C (1988b) The inhibition of cat lateral superior olive unit excitatory responses to binaural tone bursts. I. The transient chopper response. J Neurophysiol 59:164–183

Tsuchitani C, Boudreau JC (1966) Single unit analysis of cat superior olive S segment with tonal stimuli. J Neurophysiol 29:684–697

Zacksenhouse M, Johnson DH, Williams J, Tsuchitani C (1998) Single-neuron modeling of LSO unit responses. J Neurophysiol 79:3098–3110

Zhou Y, Colburn HS (2010) A modeling study of the effects of membrane afterhyperpolarization on spike interval statistics and on ILD encoding in the lateral superior olive. J Neurophysiol 103:2355–2371